AIP | Applied Physics Letters

Resistance to edge recombination in GaAs-based dots-in-a-well solar cells

Tingyi Gu, Mohamed A. El-Emawy, Kai Yang, Andreas Stintz, and Luke F. Lester

Citation: Appl. Phys. Lett. **95**, 261106 (2009); doi: 10.1063/1.3277149
View online: http://dx.doi.org/10.1063/1.3277149
View Table of Contents: http://apl.aip.org/resource/1/APPLAB/v95/i26
Published by the American Institute of Physics.

Resistance to edge recombination in GaAs-based dots-in-a-well solar cells

Tingyi Gu,[a] Mohamed A. El-Emawy, Kai Yang, Andreas Stintz, and Luke F. Lester[a]
Center for High Technology Materials, The University of New Mexico, 1313 Goddard SE, Albuquerque, New Mexico 87106, USA

(Received 8 October 2009; accepted 3 December 2009; published online 30 December 2009)

Insensitivity to edge recombination is observed in GaAs-based InAs/InGaAs quantum dots-in-a-well (DWELL) solar cells by comparing its current-voltage (*IV*) plot to GaAs control samples. The edge recombination current component is extracted by analyzing devices of different areas and then compared to DWELL cells of comparable dimensions. The results demonstrate that GaAs-based solar cells incorporating a DWELL design are relatively insensitive to edge recombination by suppressing lateral diffusion of carriers in the intrinsic layer, and thus promising for applications that require small area devices such as concentration or flexible surfaces. © *2009 American Institute of Physics*. [doi:10.1063/1.3277149]

Recent interest in using InAs quantum dots in the absorbing region of solar cells has focused primarily on the predicted increase in quantum efficiency due to the intermediate band effect or the ability to increase short circuit current density (J_{SC}) by extending the absorption edge further into the infrared range.[1–4] However, relatively little attention has been paid to the unique carrier transport properties that are introduced into the device by the dots. It is well known that quantum dot (QD) structures efficiently confine carriers and thus inhibit the lateral spreading of current to the perimeter of a device where edge recombination can dominate.[5] Consequently, QD solar cells are potentially insensitive to the edge or surface recombination current that would normally set a floor on the minimum cell area. This letter examines the phenomena by comparing the light/dark current behavior of "dots-in-a-well" (DWELL) cells[6–8] and GaAs control cells of varying area. Combined with the known insensitivity of dots to temperature,[9] the results are promising for concentration and flexible surface applications for which shrinking the size of the device and maintaining high charge collection efficiency are of paramount importance.[10]

A schematic diagram of the InAs/$In_xGa_{1-x}As$ DWELL solar cell grown by molecular beam epitaxy (MBE) is illustrated in the inset of Fig. 1. The advantages of the DWELL approach have been discussed elsewhere.[6–8] The six DWELL layers consist of InAs QDs that are sandwiched between InGaAs thin films which are placed within a 200 nm intrinsic GaAs region inside a *pin* diode. The sample is then topped with a 50 nm window layer, where the high quality MBE growth minimizes interface state density under the window layer. The total dot density is approximately 6×10^{11} cm^{-2}. The GaAs control wafer consists of the same pin configuration but without the DWELL structure in the intrinsic region.

The control and DWELL samples were fabricated simultaneously to minimize process variation. The Ge/Au/Ni/Au emitter metallization creates the solar cell finger grid and is laid out in three different areal dimensions (5×5, 3×3, and 2×2 mm^2). The bottom Ti/Pt/Au *p*-type contact is common for the solar cells on the sample. A 270-nm deep mesa, which reaches the intrinsic region, is dry-etched by inductively-coupled plasma to separate neighboring solar cells with an isolation resistance of $\sim10^5$ Ω. The mesa is deliberately shallow which minimizes the device sidewall and potential recombination there. However, the shallow mesa exposes the device to lateral diffusion current that expands the perimeter of the cell around the *i*-region and nearby base. This process results in proportionally more of the current crowding at the edge of the device, even for the emitter. The DWELL structure inhibits this lateral diffusion, whereas the GaAs control cell does not.

For *IV* characterization, the cell is illuminated using an ABET Technologies 150 W Xe lamp. A filter is inserted between source and cell to simulate the AM1.5 G spectrum. The solar cell is connected to Hewlett Packard 4155 B parameter analyzer by a four-point probe approach to eliminate the series resistance introduced by the probes and the parameter analyzer. As shown in Fig. 1, the typical DWELL device exhibits higher J_{SC} while maintaining the same open circuit voltage (V_{OC}) for smaller areas. For the GaAs control cells, however, smaller size, which has a higher perimeter-to-area ratio, makes edge recombination current dominant in these devices, and, thus, severely impacts their V_{OC} and efficiency. Here V_{OC} of the 2×2 mm^2 GaAs cell is 10% lower than the

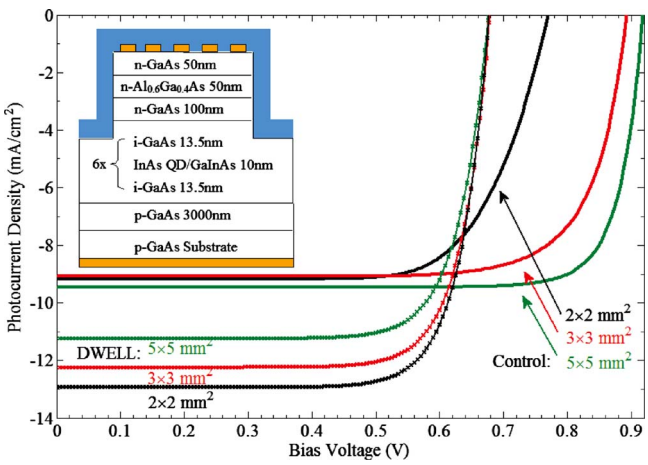

FIG. 1. (Color online) Photocurrent of DWELL and GaAs control cell of different sizes (2×2, 3×3, and 5×5 mm^2) under AM 1.5 global illumination. The inserted picture is the schematic diagram of the DWELL solar cell with six-stacks of InAs QDs embedded in InGaAs quantum wells.

[a]Electronic addresses: luke@chtm.unm.edu (Prof. Luke Lester) and tg@2342@columbia.edu.

TABLE I. Measured short circuit current densities (J_{sc}), open circuit voltages (V_{oc}), and efficiencies of the GaAs control cells and InAs DWELL solar cells under AM 1.5 G illumination.

Size	J_{sc} (mA/cm^2)		V_{oc} (V)		Efficiency (%)	
	Control	DWELL	Control	DWELL	Control	DWELL
5×5 mm^2	9.46	11.23	0.914	0.665	8.85	7.04
3×3 mm^2	9.08	12.23	0.89	0.67	7.61	7.79
2×2 mm^2	9.17	12.93	0.834	0.675	7.41	8.17

5×5 mm^2 one as shown in Fig. 1 and Table I.

To investigate the underlying physics of the V_{OC} degradation in the control samples, the dark *IV* is measured and the carrier recombination mechanism is analyzed. The conventional single diode model is[11]

$$J_d = J_0\left\{\exp\left[\frac{V}{n(V)V_t}\right]-1\right\}, \tag{1}$$

where J_d and V are the measured dark current density and voltage bias, respectively. J_0 and $n(V)$ are the bias-dependent reverse saturation current density and local ideality factor, respectively. V_t is the thermal voltage of 0.0259 V and is constant during the experiment. When $J_0 \ll J_d$, and background radiation is negligible, the local ideality factor can be approximated as

$$n(V) = \frac{d(V/V_t)}{d[\ln(I)]}. \tag{2}$$

The ideality factors for both control and DWELL cells are measured as shown in Figs. 2(a) and 2(c). Substantial differences between the GaAs and DWELL cells include the shoulder in the GaAs cells' *IV* curve and resulting hump in the $n(V)$. Neither of these effects is observed for any area in the DWELL cells. The peak in the ideality factor is more significant as the area of the GaAs cell decreases, which suggests that edge recombination is significant. Another series of wafer growths and processing produced the same results. This strongly voltage-dependent ideality factor can be modeled by the pinning of the Fermi level to surface states at the device perimeter.[12–15]

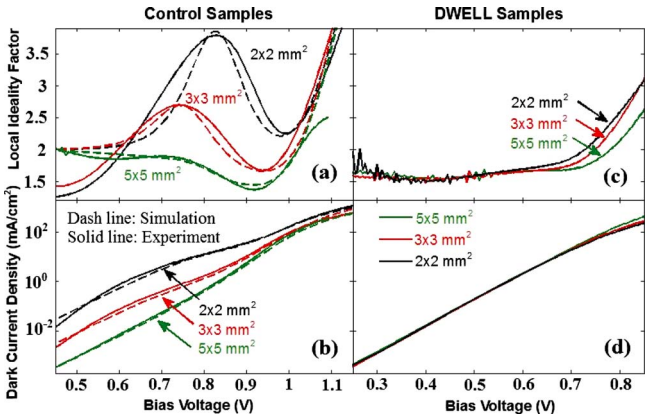

FIG. 2. (Color online) A comparison of the dark behavior of GaAs control and DWELL cells for the same dimensions (2×2, 3×3, and 5×5 mm^2). (a) Measured and simulated local ideality factor for the control cells, (b) Measured and simulated semi-logarithmic dark current density for the control cells, (c) Tested local ideality factor, and (d) Dark current density for DWELL cells. The simulation is based on Eq. (3), where the parameters extracted by curve fitting are illustrated in Table II.

After taking the edge recombination and series resistance into account, the total dark current expression can be adjusted from Eqs. (1) to (3)

$$J_d = J_b + J_p, \tag{3a}$$

$$J_b = J_{b0}\exp\left(\frac{V - J_d\times A\times R_s}{n_b V_t}\right), \tag{3b}$$

$$J_p = q\frac{n_s p_s - n_i^2}{(n_s+n_l)/S_{p0} + (p_s+p_l)/S_{n0}}\times d\times\frac{P}{A}, \tag{3c}$$

where J_b and J_p are contributions from bulk and perimeter of the cell, respectively. The fitting parameters for this model used to simulate the data in Figs. 2(a) and 2(b) are described in Table II. J_b follows the conventional diode equation and J_p is modeled using Shockley–Read–Hall (SRH) statistics as expressed in Eq. (3c).[16] It is assumed that the ideality factor (n_b) and reverse saturation current density (J_{b0}) of the bulk diode are constants over the bias range where SRH recombination dominates. The surface carrier density (p_{s0}, n_{s0}) influences the peak location of the hump in the ideality factor in Fig. 2(a), and the surface recombination

TABLE II. Parameters used in curve-fitting control samples using SRH statistics.

	Descriptions	2×2 mm^2	3×3 mm^2	5×5 mm^2
n_i	Intrinsic carrier density (cm^{-3})		1.8×10^6	
dn	Injected carrier density (cm^{-3})		$n_i\exp(V/2/V_t)$	
n_b	Ideality factor for bulk		1.31	
J_{b0}	Reverse saturation current density for bulk (mA/cm^2)		1.2×10^{-10}	
S_{p0}	Holes' surface recombination rate (cm/s)	0.8×10^7	1.0×10^7	1.0×10^7
S_{n0}	Electrons' surface recombination rate(cm/s)	7×10^7	3×10^7	2×10^7
p_{s0}	Surface holes density (cm^{-3})	6×10^{13}	1×10^{13}	3×10^{13}
n_{s0}	Surface electrons density (cm^{-3})		n_i^2/p_{s0}	
R_s	Series resistance (Ω)	2.2	1.0	0.6
$d\times P/A$	Exposed edge surface to top area ratio	1.0×10^{-5}	5.5×10^{-6}	2.5×10^{-6}
p_s	Bias-dependent surface hole density (cm^{-3})		$p_{s0}+dn$	
n_s	Bias-dependent surface electron density (cm^{-3})		$n_{s0}+dn$	
n_l, p_l	Electron, hole doping density (cm^{-3})		negligible	

rate (S_{p0}, S_{n0}) determines the shape of the hump. At high bias (>0.8 V), the series resistance (R_s) dominates the trend. Based on these features, the model is adjusted to fit the tested ideality factor and dark current density [Figs. 2(a) and 2(b)].

Good agreement is achieved between the model and the data for Figs. 2(a) and 2(b). It is found that the edge recombination current is proportional to the perimeter of the cell, while the bulk current scales with the cell area. Therefore, as predicted by the simulation and confirmed experimentally, the smaller cells, which have a comparatively larger P/A ratio, are more susceptible to the edge recombination phenomenon. Any minor disagreement between the experiment and model can be explained by our assumption that there is uniform edge recombination current across the device perimeter and that n_b and J_{b0} are constants. The edge recombination component has been simplified to a one-dimensional model with constant etched depth and surface states over the exposed perimeter. In reality, however, the recombination current is most intense near the contact fingers and decreases with distance away from the metal edges. This was verified by two-dimensional electroluminescence of the device and a SILVACO ATLAS simulation.

Although the DWELL and GaAs control cell were processed in the same run, the humps in the ideality factor disappear completely in all of the DWELL cells as demonstrated in Fig. 2(c). Similar to previously published observations,[5] the DWELL structure is effective at blocking lateral current flow to the device perimeter where surface recombination can occur. Although the dark current densities of the DWELL cells are generally higher, the values seen in the controls would have been observable in the DWELL devices. Thus, the overlapping *IV* curves shown in Fig. 2(d) for different size DWELL devices further supports the idea that the dots play an effective role in suppressing lateral diffusion of carriers.

In summary, compared to GaAs pin diode cells that experimentally display degradation of the dark current and ideality factor as the device perimeter/area ratio is increased, solar cells with an InAs/InGaAs DWELL structure positioned in the intrinsic region do not exhibit this problem. The strong peaking of the ideality factor in the GaAs control cells has been theoretically explained by a model that includes bulk and edge recombination effects. Since a hump in the ideality factor of the DWELL cell is completely absent, it is concluded that the DWELL structure limits lateral current movement and subsequent edge recombination. The DWELL devices should be especially useful for concentrated and flexible solar applications for which small area devices are highly desirable.

This work was supported in part by Dr. Kitt Reinhardt of the Air Force Office of Scientific Research under Grant No. FA9550-06-1-0407 and the Micro-Autonomous Systems Technology (MAST) program administered by the U.S. Army Research Laboratory.

[1] A. Luque, A. Marti, and L. Cuadra, IEEE Trans. Electron Devices **50**, 447 (2003).
[2] R. B. Laghumavarapu, M. El-Emawy, N. Nuntawong, A. Moscho, L. F. Lester, and D. L. Huffaker, Appl. Phys. Lett. **91**, 243115 (2007).
[3] S. M. Hubbard, C. D. Cress, C. G. Bailey, R. P. Raffaelle, S. G. Bailey, and D. M. Wilt, Appl. Phys. Lett. **92**, 123512 (2008).
[4] S. M. Hubbard, R. Raffaelle, R. Robinson, C. Bailey, D. Wilt, D. Wolford, W. Maurer, and S. Bailey, Mater. Res. Soc. Symp. Proc. **1017**, 13 (2007).
[5] D. P. Popescu, P. G. Eliseev, A. Stintz, and K. J. Malloy, J. Appl. Phys. **94**, 2454 (2003).
[6] A. Stintz, G. T. Liu, A. L. Gray, R. Spillers, S. M. Delgado, and K. J. Malloy, J. Vac. Sci. Technol. B **18**, 1496 (2000).
[7] G. T. Liu, A. Stintz, H. Li, K. J. Malloy, and L. F. Lester, Electron. Lett. **35**, 1163 (1999).
[8] S. Raghavan, P. Rotella, A. Stintz, B. Fuchs, and S. Krishna, Appl. Phys. Lett. **81**, 1369 (2002).
[9] M. Sugawara and M. Usami, Nat. Photonics **3**, 30 (2009).
[10] C. Algora, E. Ortiz, I. Rey-Stolle, V. Díaz, R. Peña, V. Andreev, V. Khvostikov, and V. Rumyantsev, IEEE Trans. Electron Devices **48**, 840 (2001).
[11] S. O. Kasap, *Optoelectronics and Photonics: Principles and Practices* (Prentice Hall, Englewood Cliffs, NJ, 2006) p. 262.
[12] M. D. Abbott, J. E. Cotter, T. Trupke, and R. A. Bardos, Appl. Phys. Lett. **88**, 114105 (2006).
[13] P. E. Dodd, T. B. Stellwag, M. R. Melloch, and M. S. Lundstrom, IEEE Trans. Electron Devices **38**, 1253 (1991).
[14] K. R. McIntosh and C. B. Honsberg, Proceedings of the 16th European Photovoltaic Solar Energy Conference, Glasgow, UK, 2000 (unpublished).
[15] S. J. Robinson, S. R. Wenham, P. P. Altermatt, A. G. Aberle, G. Heiser, and M. A. Green, J. Appl. Phys. **78**, 4740 (1995).
[16] W. Shockley and W. T. Read, Phys. Rev. **87**, 835 (1952).